HHS Public Access

Author manuscript

Dev Biol. Author manuscript; available in PMC 2017 January 25.

Published in final edited form as:

Dev Biol. 2017 January 15; 421(2): 219–232. doi:10.1016/j.ydbio.2016.11.016.

Distinct requirements of *wls*, *wnt9a*, *wnt5b* and *gpc4* in regulating chondrocyte maturation and timing of endochondral ossification

Irving TC Ling[a,c], **Lucie Rochard**[a], and **Eric C. Liao**[a,b,*]

[a]Center for Regenerative Medicine, Massachusetts General Hospital, Shriners Hospital for Children, Harvard Medical School, Boston, MA 02114, USA

[b]Division of Plastic and Reconstructive Surgery, Massachusetts General Hospital, Boston, MA 02114, USA

[c]School of Medicine, Veterinary and Life Sciences, Glasgow University, UK

Abstract

Formation of the mandible requires progressive morphologic change, proliferation, differentiation and organization of chondrocytes preceding osteogenesis. The Wnt signaling pathway is involved in regulating bone development and maintenance. Chondrocytes that are fated to become bone require Wnt to polarize and orientate appropriately to initiate the endochondral ossification program. Although the canonical Wnt signaling has been well studied in the context of bone development, the effects of non-canonical Wnt signaling in regulating the timing of cartilage maturation and subsequent bone formation in shaping ventral craniofacial structure is not fully understood.. Here we examined the role of the non-canonical Wnt signaling pathway (*wls, gpc4, wnt5b* and *wnt9a*) in regulating zebrafish Meckel's cartilage maturation to the onset of osteogenic differentiation. We found that disruption of *wls* resulted in a significant loss of craniofacial bone, whereas lack of *gpc4, wnt5b* and *wnt9a* resulted in severely delayed endochondral ossification. This study demonstrates the importance of the non-canonical Wnt pathway in regulating coordinated ventral cartilage morphogenesis and ossification.

Keywords

Wnt; Chondrocyte; Osteoblast; Zebrafish; Meckel's cartilage; Endochondral ossification

*Corresponding author at: Center for Regenerative Medic ine, Massachusetts General Hospital, Shriners Hospital for Children, Harvard Medical School, Boston, MA 02114, USA. cliao@partners.org (E.C. Liao).

Author contributions

IL designed and performed experiments, analyzed the data and wrote the manuscript. This work is submitted as part of IL doctorate thesis.

LR helped with experimental design, analyzed the data and edited the manuscript.

ECL supervised the work, supervised with experimental design, data analysis and carried out manuscript preparation.

1. Introduction

Cranial neural crest cells (NCC) are assembled into cartilaginous structures that prefigure development of the craniofacial skeleton (Eames et al., 2012; Hammond and Schulte-Merker, 2009; Kague et al., 2012; Olsen et al., 2000; Paul et al., 2016). After migrating into the first (mandibular) and second (hyoid) pharyngeal arches, CNCCs give rise to a series of cartilaginous anlage (Mork and Crump, 2015). Meckel's cartilage is a first pharyngeal arch derivative that is considered a scaffold and template for mandibular development. The mandible develops in two distinct steps; first through intramembranous ossification supported by the body of the Meckel's cartilage followed by endochondral or perichondral ossification of the distal and proximal regions (hereafter referred to as endochondral) (Eames et al., 2013; Frommer and Margolies, 1971; Savostin-Asling and Asling, 1973). In zebrafish, the mentomeckelian (distal midline) and retroarticulars (proximal jaw joint) form through endochondral ossification while the dentary bone (body) form through intramembranous ossification (Eames et al., 2013). Other craniofacial bones that undergo endochondral ossification include the ceratohyal and the ceratobranchials (Hammond and Schulte-Merker, 2009; Paul et al., 2016; Schilling and Kimmel, 1994, 1997).

The majority of the craniofacial bones, including the mandibular bone are CNCC-derived unlike the bones from the limbs and trunk that are mesoderm-derived. Despite the histological similar appearance of the mesoderm- and CNCC-derived bones, the CNCC-derived bones of the jaw for example differ biologically; they possess distinct gene expression signatures, higher alkaline phosphatase activity, higher proliferation and greater regenerative capabilities (Heuze et al., 2014; Hochgreb-Hagele et al., 2015; Ichikawa et al., 2015; Quarto et al., 2010). Identifying the role of local signaling pathways that help to properly develop these cartilage structures is critical to the understanding of the precise shape and size that bones acquire, a requisite for their function.

The Wnt signaling pathway family members have been shown to be important in regulating bone formation, maintenance and remodeling (Olsen et al., 2000; Rodda and McMahon, 2006). Canonical Wnts have been extensively studied in bone biology and demonstrated that the Wnt/β-catenin signaling is important for mesenchymal precursor cells to differentiate into chondrocyte or osteoblast lineages during skeletogenesis (Day et al., 2005; Rodda and McMahon, 2006). Loss- and gain-of function studies have highlighted the requirement for β-catenin to repress chondrogenesis by favoring osteogenesis and playing a vital role in bone homeostasis through regulating the balance between osteoblastic and osteoclastic activity (Day et al., 2005; Hill et al., 2005). However, there are many other Wnts (*e.g.* Wnt4, Wnt5, Wnt11) that act through a non-canonical Wnt (β-catenin independent) pathway, to regulate cell polarity and migration during embryonic development (Semenov et al., 2007). In chick, ectopic *Wnt5a* expression led to a delay in chondrocyte differentiation while ectopic *Wnt4* promoted differentiation (Hartmann and Tabin, 2000). Overexpression of *Wnt14* (currently named *Wnt9a*) in chick limbs led to ectopic joint formation (Hartmann and Tabin, 2001). In murine long bones, endogenous *Wnt5a* and *Wnt5b* regulate endochondral skeletal development by coordinating chondrocyte proliferation (Yang et al., 2003). In zebrafish, non-canonical Wnts (Wnt4a, Wnt11r, Wnt5b, Wnt9a, Wnt11) have been shown to play a key role in early and late craniofacial patterning from the formation of pharyngeal pouches to the

patterning and shaping of cartilaginous-structures (Choe et al., 2013; Curtin et al., 2011; Heisenberg et al., 2000; Sisson et al., 2015). These studies highlight the importance of non-canonical Wnt in skeletal development. But, how non-canonical Wnt ligands exert their function during cartilage maturation and ossification remains to be explored.

To determine the role of non-canonical Wnt in craniofacial development, we generated and analyzed different mutants involved at various steps of the non-canonical Wnt signaling pathway; *wls* and *gpc4* (Wnt trafficking proteins) and *wnt9a* and *wnt5b* (ligands) (Sisson et al., 2015; Topczewski et al., 2011). Our study focused on the cellular events occurring during Meckel's cartilage morphogenesis and ossification. We demonstrated, for the first time, that different Wnt genes have regional-specific requirements during Meckel's cartilage development. Further, we showed that Wnt signaling is required for timely cartilage maturation and for the onset of the endochondral ossification program.

2. Results

2.1. *wls*, *wnt9a*, *wnt5b* and *gpc4* are expressed in discrete regions of the ventral craniofacial structures

Previous studies have showed that *wls, wnt9a, wnt5b* and *gpc4* are expressed in ventral cartilage elements at the early time points of 55 h post-fertilization (hpf) and 72 hpf (Curtin et al., 2011; Rochard et al., 2016; Sisson et al., 2015). Sisson et al. showed that *gpc4* is expressed in the pharyngeal endoderm, neural crest and mesoderm while *wnt5b* is restricted to the neural crest and mesoderm (Sisson et al., 2015). To understand the role of these genes in early ossification, we analyzed their gene expression at a later craniofacial developmental stage by performing whole-mount RNA *in situ* hybridization (WISH) at 96 hpf time point, which is when ventral craniofacial cartilage structures have formed and ossification is initiated.

wls, *wnt9a* and *gpc4* transcripts were detected in the mesenchyme surrounding the chondrocytes of the ventral cartilage structures, with *wls*, *wnt9a* and *wnt5b* transcripts localized anteriorly as shown in Fig. 1. Expression of *wls*, *wnt5b* and *gpc4* are observed at the jaw joint (Fig. 1A, C, D, arrowhead). *wnt5b* and *wls* transcripts are co-localized to the oral epithelium (Fig. 1A, C, black arrowhead) while *wnt9a* expression pattern is restricted to the midline of Meckel's cartilage (Fig. 1B, arrowhead). *wnt5b* expression was observed within the ceratobranchials and mouth opening epithelium (Fig. 1C). These detailed delineations of gene expressions fill-in important previously published expression patterns and can provide us with greater insight into their role in craniofacial development.

2.2. Loss of Wnt signaling leads to abnormal Meckel's cartilage chondrocyte arrangement

Prior analyses indicated significant shortening of Meckel's cartilage in *wls, wnt5b* and *gpc4* mutant lines and loss of Meckel's and ventral cartilages in *wnt9a* morphants (Curtin et al., 2011; Sisson et al., 2015; Wu et al., 2015). To gain better understanding of Meckel's cartilage development, we performed a systematic and detailed analysis of Meckel's in each of these existing mutants. Craniofacial structures were stained with Alcian blue and the length/width (L/W) ratio of Meckel's cartilage was analyzed (Fig. 2A). At 96 hpf, wild-type

(WT) embryos have a larger mean L/W ratio of 0.804 ± 0.019 which was statistically significant compared to *wls*, *wnt5b* and *gpc4* mutants; 0.566 ± 0.033, 0.447 ± 0.029, 0.542 ± 0.048 respectively (L/W ± standard deviation; $p < 0.01$ Kruskal-Wallis test with Dunn's multiple comparisons test; Fig. 2B, D, E, P). We did not observe a statistical difference in *wnt9a* mutants (0.756 ± 0.104; n=10, p=0.125) however; its prominent open-mouth phenotype prompted us to examine differences in phenotype across the Wnt mutants (Fig. 2C). It is important to note that these morphological differences were not due to cell number differences, as chondrocyte count was not statistically significant amongst the different mutants (p=0.1151, One-way ANOVA; Fig. 2Q). These results, coupled with the gene expression data illustrate that Wnt signaling is essential for morphogenesis of ventral craniofacial cartilages during zebrafish embryogenesis.

2.3. Cellular organization reveals two distinct zones in Meckel's cartilage: midzone and body

To understand the morphologic phenotype displayed by the Wnt mutants, the L/W of Meckel's cartilage and the individual cell sizes was followed during Meckel's cartilage morphogenesis. We performed live confocal imaging of each mutant using the Tg(*sox10*:GFP) line and tracked the L/W measurement from the earliest time Meckel's cartilage forms a distinguishable structure (55 hpf) to the time point when the arch is fully formed (96 hpf) (Eames et al., 2013) (Fig. 3A–E).

In WT embryos, Meckel's cartilage L/W ratio grew from 0.28 ± 0.01 to 0.78 ± 0.10 with a period of accelerated extension occurring between 55 and 72 hpf. In *wls*, *wnt9a* and *wnt5b* mutants, the Meckel's cartilage appeared to extend at a similar rate between 55 and 60 hpf but abnormalities were evident at 72 hpf (Fig. 3F). *gpc4* mutants displayed the slowest extension of Meckel's cartilage with defects observed as early as 60 hpf (Fig. 3E). Meanwhile, extension rate in *wnt9a* mutants appeared normal (Fig. 3C).

In addition to the altered global dimensions of Meckel's cartilage, we observed two morphologically distinct regions: the midzone (Fig A, 96 hpf purple box) and the body (Fig. 3A, 96 hpf white box) that differed in cell size and organization. In WT embryos, cells within the body were seen to stack and elongate, in contrast to the chondrocytes within the midzone remained smaller and cuboidal at 72 hpf. By 96 hpf, cells within the midzone acquired a more columnar shape with a L/W of 2.53 ± 0.35 and stacked to align with cells within the body that have a L/W of 4.47 ± 0.56.

In *wls*, *wnt9a* and *gpc4* mutants, chondrocytes within the midzone at 96 hpf failed to align and remained small and cuboidal with a L/W of 1.31 ± 0.05, 1.36 ± 0.14 and 1.51 ± 0.25 respectively. However, *wls* and *wnt9a* mutants displayed columnar cells within the body (3.74 ± 0.59 and 3.66 ± 0.34 respectively) compared with *gpc4* where cells remained significantly smaller and rounded (1.88 ± 0.24) (Fig. 3D, G, H). In *wnt5b* mutant, there was some degree of alignment of the cells within the midzone but cells were also smaller compared to WT in both the midzone and the body (1.93 ± 0.33 and 2.90 ± 0.37 respectively) (Fig. 3E, G, H).

These studies suggested that there are two distinct morphologic zones in Meckel's cartilage that differ in cell shape, organization and Wnt signal requirement.

2.4. Wnt signaling is required for chondrocyte polarity in Meckel's cartilage

Given the differential requirement observed by the chondrocyte morphology and organization between the midzone and body regions of Meckel's cartilage, we examined whether chondrocyte polarity is differentially disrupted differently between the *wls, wnt9a, wnt5b* and *gpc4* mutants. Chondrocyte polarity was visualized using acetylated-alpha tubulin to mark microtubule-organizing centers (MTOC) indicative of primary cilia, at 3.5 days post fertilization (dpf), a time point when all Wnt mutants displayed distinct abnormalities between the midzone and the body (Fig. 3) (Sepich et al., 2011).

In WT embryos, the primary cilia were aligned to the center of the cell following the curve of the Meckel's arch. In addition, cell polarity staining revealed three apparent zones of uniform polarity with 2 inflection points of the primary cilia, which we named here as points A and B (Fig. 3I, N). Point A was observed to be at the anterior midline and point B was located at a position that has been observed to provide musculoskeletal attachment and pre-osteoblast condensation (Fig. 3I). In contrast, all Wnt mutants displayed disorganized primary cilia arrangements in the midzone resulting in a malformed midzone and loss of the Meckel's cartilage arch shape (Fig. 3J–M). In all mutants, chondrocyte polarity appeared to be randomized and inflection at points A and B were not detected.

We measured the angle at which the MTOC were positioned within the midzone of Meckel's cartilage (Fig. 3T). In WT embryos, 76.3% of cells had primary cilia oriented in a narrow distribution along the x-axis in the proximal (0°) and distal (180°) directions (red boxes, Fig. 3O). This organized pattern was lost in all Wnt mutants as their chondrocytes localized primary cilia were randomly positioned without restriction about the X-axis (Fig. 3P–S). Thus, Wnt signaling is required for primary cilia organization in the midzone of Meckel's cartilage.

2.5. Wnt is required for timely bone ossification

Considering that the anatomic location of point B may coincide with osteoblast condensation and musculoskeletal attachment, we explored how the loss of polarity and cartilage morphological defects affect bone development in *wls, wnt9a, wnt5b* and *gpc4* mutants. Embryonic bone development occurs as early as 3 dpf in zebrafish, permitting analysis of ossification events in *wls*, *wnt9a*, *wnt5b* and *gpc4* mutants that typically survive until 12–15 dpf (Bird and Mabee, 2003). Bone phenotype at two time points were compared in order to ascertain the dynamic changes of ossification: 1) 4 dpf when cartilage elements have established their structures and 2) 8 dpf when most craniofacial bones (both intramembranous and endochondral) have initiated ossification, evidenced by Alizarin red staining. We did not include 12–15 dpf analyses to avoid inconclusive phenotype of a dying embryo.

At 4 dpf, WT embryos started to develop intramembranous bones (Fig. 4U diagram-in red); dentary, branchiostegal rays, opercle, and cleithrum (Fig. 4A). By 8 dpf, the endochondral bones (orange Fig. 4U); ceratohyal, mentomeckelian, retroarticular and ceratobranchial-5

started to form ossification and the previously noted intramembranous bones grew in size (Fig. 4F). The positions of these bones correlated with the expression of late and early ossification markers, *osteocalcin*, a marker of mature osteoblast (green in Fig. 4K) and *osterix*, a marker of osteoblast (Singh et al., 2012) (red in Fig. 4P).

In *wls* mutants, only the opercle and cleithrum formed at 4 dpf, remaining unchanged at 8 dpf (n=25). This argues against developmental delay as we would expect a greater number of bones to have started to develop between these two time points as observed in WT. The lack of ossification in the *wls* mutant correlated with the loss of expression of the bone specific markers: *osteocalcin* (green in Fig. 4L) and *osterix* (red in Fig. 4Q). It is important to note that larvae at 8 dpf were examined from confocal stacks in WT and mutants in the Tg(*ocn*:GFP;*sox10*:mCherry) and Tg(*osx*:mCherry;*sox10*:GFP) reporter backgrounds, where it is clear that the Meckel's cartilage is developed but dysmorphic, providing additional morphologic data to support that the lack of ossification is not due to developmental delay. These results suggested that in the *wls* mutant osteoblasts not only failed to secrete bone matrix as indicated by the absence of Alizarin red stain, but also failed to differentiate into mature osteoblasts.

Despite the opened mouth phenotype in *wnt9a* mutants, all intramembranous bones formed appropriately at 4 dpf (Fig. 4C) and grew normally in size and shape similar to WT embryos by 8 dpf (Fig. 4H). *wnt5b* mutant also displayed a similar appearance of larval cranial bone elements as *wnt9a* mutant (Fig. 4D, I, N, S). However, in both mutants, *wnt9a* and *wnt5b*, the majority of abnormalities were seen within the endochondral bones; mentomeckelian (n=0/11 and n=0/18), retroarticular (n=0/11 and n=4/18), ceratobranchial 5 (n=1/11 and n=0/18) and ceratohyal bones (n=6/11 and n=7/18) (summary in graph; Fig. 4V). High-resolution images of Alizarin red staining in WT reveals a thin, flat perichondral bone, termed the mentomeckelian that is distinct from the thicker dentary bone (Fig. 4K). A clear boundary at 8 dpf helps differentiate the two bones, allowing quantification and analysis. *wnt9a*, *wnt5b* and *gpc4* all lack the mentomeckelian despite staining for the dentary (Fig. 4M–O). *wls* completely lacks both the dentary and mentomeckelian (Fig. 4L). Double transgenic line with *sp7*:GFP and *sox10*:mCherry at 8 dpf shows a perichondral cell expressing *sp7* (Supplementary Fig 2). This cell is observed directly adjacent to the perichondrial cells as oppose to the *sp7* positive cells of the dentary lying above the perichondrium.

Expressions of *osterix* and *osteocalcin* in *wnt9a* and *wnt5b* mutants show a reduction in the number of mature osteoblasts compared to WT in structures where endochondral bone occurs (Fig M, N, R, S). In *gpc4* mutants, a similar bone phenotype as described for *wls* mutants at 4 dpf with only the opercle and cleithrum present. Interestingly, despite a more severe Meckel's cartilage shortening, all bones that formed intramembranously were detected by 8 dpf in the *gpc4* mutants (Fig. 4E). This correlated with *osterix* and *osteocalcin* expressions (Fig. 4J, O). However, similar to the *wnt9a* and *wnt5b* mutants, defects were observed by the absence of endochondral bone in all *gpc4* mutant embryos imaged (n=12; Fig. 4Q). Furthermore, endochondral bones were not detected in *gpc4* mutants even when observed at 8 dpf.

Taken together, these results showed that *wls* is required for both intramembranous and endochondral ossification while *wnt9a, wnt5b* and *gpc4* are required only for endochondral ossification as evident by the loss of differentiation of ventral chondrocytes to osteogenic progenitors. In addition, ossification can occur despite significant Meckel's cartilage dysmorphology as seen in *gpc4* mutant. When *wls* requirement for ossification is considered in the context of intramembranous ossification that are present in *wnt9a* and *wnt5b* mutants, it is likely that other ligands require *wls* for its secretion and function in direct osteogenesis from NCC progenitors.

2.6. Cartilage joint and muscle defects in *wls*, *wnt9a*, *wnt5b* and *gpc4* mutants

In addition to cartilage formation, shaping the craniofacial structures requires properly formed joints and muscles. In zebrafish, the jaw and hinge joints are the two major joints in the craniofacial region. We examined the retroarticular and coronoid process of Meckel's cartilage that articulates with the palatoquadrate to form the jaw joint and the interhyal that forms a sesamoid-like bone between the ceratohyal and hyosymplectic.

Alcian blue staining at 8 dpf revealed marked joint defects in *wls*, *wnt9a, wnt5b,* and *gpc4* mutants (Fig. 5B, C, E). The magnified view showed that in *wls*, *wnt9a* and *gpc4* mutants, there is a significantly reduced number of chondrocytes within the interhyal bone at the hinge joint (Fig. 5B′–E′ right). In addition, the retroarticular process in *wls* and *gpc4* mutants were significantly malformed and shortened (Fig. 5L) compared to WT ($p < 0.0001$ for both).

Due to evidence highlighting the role of muscles in maintaining joint integrity, the craniofacial muscles in our Wnt mutants were observed (Shwartz et al., 2012). Wnt embryos in Tg(*sox10*:GFP) background were stained with phalloidin, a toxin used to visualize actin filaments (Fig. 5F–J). The staining suggests that *wls* and *wnt5b* mutants have normal muscle appearance and pattern, although both exhibited some muscle shortening likely secondary to the craniofacial cartilage dysmorphologies (Fig. 5G–I). Interestingly *wnt9a* mutants did not appear to have any overt muscle defects, which was surprising since we expected that muscle defects would affect mouth opening. The most severe muscle defect was observed in *gpc4* mutants where the intermandibularis posterior muscle that normally attaches to the Meckel's cartilage appeared disorganized and invaded ectopic gaps between the chondrocytes (Fig. 5J, white arrows). The muscle defect in *gpc4* mutants may explain the more severe Meckel's cartilage length/width ratio compared with *wls* mutants. These data also suggest that cranial muscles were properly specified in *wls*, *wnt9a,* and *wnt5b* mutants and they do not contribute to the cartilage morphology phenotypes. It appears that Wnt mutants may have a greater effect on neural crest cell-derived tissues, as the craniofacial muscles are mesoderm-derived.

2.7. *wls* required chondrocyte proliferation

Our data showed that abrogation of the Wnt signaling led to Meckel's cartilage malformations and that *wls*, *wnt9a*, *wnt5b* and *gpc4* have a distinct role in shaping ventral cartilage structures. For endochondral bone formation, following condensation of NCC cells to sites of future skeletal structures, subsequent proliferation of chondrocytes is key for

subsequent linear growth and enlargement. Therefore, chondrocytes undergoing mitotic division were assayed with BrdU in 6 dpf mutants to determine if Wnt mutants also affect chondrocyte proliferation.

In WT larvae, chondrocytes at 6 dpf were noted to be actively proliferating in Meckel's cartilage and the surrounding mesenchyme, consistent with previously report findings in zebrafish (Fig. 6A) (Hammond and Schulte-Merker, 2009). However, chondrocyte proliferation was most severely affected in *wls* mutants ($p < 0.0001$; Fig. 6B) compared to *wnt9a*, *wnt5b* and *gpc4* mutants. Since proliferation was decreased in *wls* at 6 dpf, we examined if NCC condensation surrounding Meckel's cartilage at 60 hpf was also affected and found no difference in positive BrdU cell in *wls* mutants compared to WT (SFig. 1A, B). Moreover, 96 hpf *wls* mutant embryos had the same number of cells within Meckel's cartilage (Fig. 2L, Q) suggesting that *wls* has a more important role later in chondrocyte proliferation, maturation and differentiation for endochondral ossification. The data also suggest that *wnt9a, wnt5b* and *gpc4* are dispensable for chondrocyte proliferation but may be required later in chondrocyte maturation.

To exclude that the lack of proliferation could be due to cell survival, we performed live acridine orange assays to evaluate cell death. There was no increase in the number of apoptotic chondrocyte or mesenchymal cells in *wls* mutant to account for the severity of the bone phenotype displayed (Fig. 6C,D).

Thus, these data suggest that *wls* is required for late proliferation of chondrocytes in Meckel's cartilage but not for cell survival. Indeed, mesenchymal expression of *wls* is necessary for the expansion and differentiation of chondrocytes to enable growth of Meckel's cartilage (Rochard et al., 2016). The data underscores the spatiotemporal regulation of Wnt signaling in ventral cartilage development.

2.8. Endochondral ossification requires non-canonical Wnt

To examine how chondrocyte differentiation is affected in the Wnt mutants, we studied the expression of genes involved at different stages of chondrogenesis by whole-mount *in situ* hybridization (WISH) in 4 dpf embryos: *sox9a* (early chondrogenesis), *col2a1, col10a1a, col1a2* (chondrocytes during early to late extracellular matrix remodeling); *runx2a* (osteoblast differentiation) and *bapx1* (joint patterning) (Eames et al., 2012; Flores et al., 2004; Miller et al., 2003; Schilling and Kimmel, 1997; Yan et al., 2002). WISH images are shown in Fig. 7 and summarized in Table 1.

By 4 dpf, *sox9a* expression was observed throughout the ventral cartilages with increased expression at the distal edges of the cartilage elements. Normal *sox9a* expression was found in *wnt9a, wnt5b* and *gpc4* mutants (Fig. 7A, C–E). However, *wls* mutant appeared to display enhanced *sox9a* expression throughout the craniofacial structures (Fig. 7B). Since *sox9a* is necessary for *col2a1* expression (Yan et al., 2002), we examined *col2a1* expression and did not detect overt difference in staining or ectopic expression across the different Wnt mutants (Fig. 7F–J).

Expression of *col10a1a* shows mature stage of hypertrophic cartilage chondrocytes. In contrast to tetrapods, zebrafish osteoblast have also been found to express *col10a1a* (Eames et al., 2012). At 4 dpf, *col10a1a* expression was observed in most craniofacial NCC-derived osteoblasts, mesoderm derived osteoblasts (parasphenoid, cleithrum) and chondrocytes in the ceratohyal adjacent to the ceratohyal bone (Fig. 7K). In *wls* mutants, only expression within the parasphenoid, opercle and cleithrum was observed (Fig. 7L). A similar pattern was observed in *wnt5b* mutants (Fig. 7N). However, *wnt9a* and *gpc4* mutants exhibited expression of *col10a1a* in the majority of the facial osteoblasts but loss of expression in the ceratohyal (Fig. 7M, O).

To examine mineralization, we looked at *col1a2* expression patterns that is expected to be expressed in mineralized bone and perichondrium, tendons and epidermis but not in chondrocytes (Eames et al., 2012). At 4 dpf, *col1a2* expression was observed in the dentary, opercle and cleithrum, the only bones that stained for Alizarin red as well (Fig. 7P) (Eames et al., 2013). No staining of the dentary was detected in *wls* or *wnt5b* mutants (Fig. 7Q, S) but expression was present in *wnt9a* and *gpc4* mutants (Fig. 7R, T). however, tendon development appeared intact since the expression of *col1a2* in the sternohyoides tendon, palatoquadrate ligament, and intermandibularis posterior tendon appeared normal in all Wnt mutants.

Expression of *runx2a* (runt-related transcription factor), a gene required for osteoblast differentiation and activation of *col1a2* transcription was used to assess early bone formation (Eames et al., 2004; Flores et al., 2004). In WT, by 4 dpf *runx2a* was expressed in all craniofacial dermal osteoblasts as well as perichondral-osteoblasts within the ceratohyal (Fig. 7U). Notably, *runx2* was consistently strongly expressed in *wls* mutants but was expressed at normal levels in *wnt9a*, *wnt5b* and *gpc4* mutants (Fig. 7V–Y).

Our Wnt mutants displayed joint defects; therefore we examined the expression levels of *bapx1* (*bagpipe*-related transcription factor), which is involved in joint specification (Miller et al., 2003; Nair et al., 2007). *bapx1* transcripts localized to the jaw joint in WT (Fig. 7Z). This pattern is preserved in *wls* and *wnt5b* mutants in addition to a smaller ventral midline domain (Fig. 7AA black arrowhead) in the hyoid arch of *wls* mutants (Fig. 7AA, AC). Interestingly, jaw joint *bapx1* expression was not detectable in *gpc4* mutants indicating a failure in patterning of the joint (Fig. 7AD) and weak in *wnt9a* mutants, which may indicate defective joint integrity (Fig. 7AB).

In summary, in all *wls* mutants observed, we noted the enhanced expression of *sox9a* and *runx2a* and interestingly, a loss of *col10a1a* and *col1a2* expression. In *wnt9a*, *wnt5b* and *gpc4* mutants, there was a loss of *col10a1a* in endochondral bones. Altogether, our data showed a defect in the differentiation process of chondrocytes in the absence of Wnt signaling, a process required for chondrogenic maturation and subsequent initiation of the endochondral ossification process.

3. Discussion

Wnt signaling pathways play important roles in craniofacial cartilage and bone development. Once chondrocytes form distinct cartilage structures, differentiated chondrocytes can either maintain their chondrogenic state to form articular cartilage or undergo hypertrophic maturation in the process of endochondral ossification (Kronenberg, 2003). The canonical Wnt/β-catenin pathway has been investigated to be key in promoting chondrogenesis, initiating chondrocyte hypertrophy and regulating osteogenesis (Day et al., 2005; Glass et al., 2005; Hill et al., 2005). However, the non-canonical pathway has been less studied. It has been shown that both the planar cell polarity (PCP) and Ca^{2+} have been shown to induce cytoskeleton reorganization, chondrocyte stacking and axial patterning (Fanto and McNeill, 2004; Le Pabic et al., 2014; Rochard et al., 2016; Sisson et al., 2015). Here we showed that the Wnt non-canonical genes; *wls*, *wnt9a*, *wnt5b* and *gpc4* each have distinct requirements in chondrogenesis and osteogenesis during craniofacial ventral cartilage development.

3.1. *wls*, *wnt9a*, *wnt5b* and *gpc4* are required for proper craniofacial cartilage and joint development

In ventral cartilage development, Wnt signaling is required for early CNCC induction and later in CNCC migration, specification and proliferation by participating in a gene regulatory network with *Edn1* and *Bmp* (Alexander et al., 2014). Heat-shock studies inhibiting Wnt through the overexpression of *dkk1, a Wnt* antagonist and *dntcf3,* a dominant negative form of the Tcf3 transcription factor, showed ventral patterning defects in the mandibular arch (Alexander et al., 2014). Recent studies using *Wls* to manipulate Wnt signaling, implicated its role in skeletal development by regulating osteogenesis and chondrogenesis (Maruyama et al., 2013; Rochard et al., 2016; Zhong et al., 2012). In zebrafish, a previous study suggested that *wls* modulates *fgf3* expression to direct cell proliferation (Wu et al., 2015). We recently highlighted the importance of *wls* in medialateral and dorsal-ventral patterning during palate morphogenesis (Rochard et al., 2016). We found that *wls* affected ventral cartilage elements similar to the ethmoid plate where Meckel's cartilage appeared shorter and chondrocytes were smaller and cuboidal. Cartilage morphologic analysis of *gpc4* and *wnt5b* mutants also recapitulated previously published work (Sisson et al., 2015). However, we noted that a later expression analysis of *gpc4* appeared in the tissues surrounding cartilage structures as oppose to an earlier expression found within the CNCC and chondrocytes. This may suggest a more dynamic modulation of *gpc4* during craniofacial development with earlier requirements in chondrogenesis and later in development of surrounding structures such as muscle cells.

When we examined cartilage structures at 8 dpf, we observed profound articular cartilage abnormalities across our *Wnt* mutants including loss of joint integrity and extension of the retroarticular process. Wnts have all been implicated in joint development through their role in articular cartilage formation (Hartmann and Tabin, 2001; Spater et al., 2006). In mice, *Wnt9a* has been shown to maintain joint integrity by suppressing chondrocyte differentiation within the joint interzones (Spater et al., 2006). *Wnt4* and *Wnt16* are expressed in joints (Guo et al., 2004; Hartmann and Tabin, 2001) and mice harboring loss of both genes; *Wnt9a* $-/-$*;Wnt4* $-/-$ developed bony fusions and synovial chondroid metaplasia of acral bones

(Spater et al., 2006). Here we showed that *wls* and *gpc4* mutants displayed the most severe joint defects. Interestingly, both have opposite *bapx1* expression patterns with *gpc4* showing a complete loss and *wls* an exaggerated level of expression pattern. *bapx1* is a downstream target of *edn1*, specifying the jaw joint by shaping and maintaining articular cartilage through the activation of *chordin* and *gdf5* (Miller et al., 2003; Nakayama et al., 2004; Storm and Kingsley, 1999). The loss of expression in *gpc4* and the overexpression seen in *wls* implies that either under or over expression levels of *bapx1* result in jaw joint malformation.

Studies in mouse have demonstrated that *Wnt9a* loss-of-function mutation is lethal at birth (Spater et al., 2006). *Wnt9a* mutant embryos displayed partial joint fusion of the carpal and tarsal joints, and shortened appendicular long bones. In addition, they showed that ectopic activation of *Wnt9a* resulted in joint induction. We previously showed that zebrafish *wnt9a* morpholino knockdown resulted in the loss of ventral cartilage structures by affecting NCC migration (Curtin et al., 2011). Here, we found that a *wnt9a* mutation is embryonic lethal as well but the phenotype appeared less severe than in mouse. Our *wnt9a* mutants were able to develop craniofacial structures but were unable to close their mouth, an anteriorly displaced Meckel's cartilage, which resulted in an inability to feed properly. Interestingly, *wnt9a's* anteriorly displaced Meckel's appears very similar to the phenotype of the *spitzmaul*^{m636} mutant previously described in a large scale mutagenesis screen that has not yet been characterized (Neuhauss et al., 1996). Further analysis shows that cells within the midzone of Meckel's cartilage were smaller, rounder and less stacked compared to WT, suggesting a distinct midline anterior role of *wnt9a* in craniofacial development. Additionally, we found that although *wnt9a* mutants have a similar L/W of Meckel's cartilage and cell L/W in the body of Meckel's compared to WT, the cell L/W at the midline is disrupted and significantly smaller. This resulted in an elongated lower jaw that is abnormally arched due to the ventral displacement of Meckel's cartilage. Indeed, previous mutants with elongated lower jaw also displayed a ventrally displaced ceratohyal, such as the *doolittle*^{m636} mutant resulting in abnormal mastication and respiration (Neuhauss et al., 1996). While we have not directly assessed for movement of the lower jaw, we observed distinct patterning differences of the interhyal in *wnt9a* and together, with low *bapx1* expression levels in *wnt9a* mutants, we believe that joint integrity may to explain this malocclusive jaw phenotype that plays crucial role in feeding.

3.2. Shaping Meckel's cartilage by Wnt

For proper shaping and patterning of Meckel's cartilage, chondrocytes must first undergo convergence, intercalation, elongation and proliferation. Thereafter, chondrocytes are required to align, stack and polarize to maintain the proper morphologic structure.

We identified two regions within Meckel's cartilage with distinct cell behaviors, the midzone and the body. In all our Wnt mutants, the cells within the midzone remained smaller and rounded throughout cartilage development, which correlated with abnormal shaping and length of Meckel's cartilage. Although cells within the body have a similar cell L/W ratio, they do not appear to stack like disc of coins as observed in WT and previously described. Our analysis of cell polarity within this midzone showed that in our Wnt mutants, the cells in the midzone were disorientated and had lost their directional polarization,

observed in WT. Our study extended the polarity map of Le Pabic et al. and found that these opposing points of polarity (Points A and B) is what gives Meckel's cartilage its unique arched shape and rounded midline pattern (Le Pabic et al., 2014). When polarity is lost, as it is in our Wnt mutants, Meckel's cartilage remains shortened and misshapen.

Interestingly *gpc4* mutants displayed the most severe Meckel's cartilage cellular anomalies with rounded cells observed in the midzone and body. We reasoned that the intermandibularis posterior muscle defect prevented cell intercalation and extension. Indeed, previous studies on chemically paralyzed mice, chick and zebrafish showed defects in cell convergence-extension and intercalation (Kahn et al., 2009; Nowlan et al., 2008; Shwartz et al., 2012). Therefore, these observations indicate that cell extension in the body of Meckel's cartilage may be partially rescued by the normal developing craniofacial muscles that drive the jaw anteriorly.

3.3. Non-canonical Wnt is required for spatiotemporal control of endochondral bone formation

Perturbations in Wnt signaling have been studied extensively with the role of the canonical Wnts in bone biology better defined (Clevers and Nusse, 2012; Hartmann, 2006; Krishnan et al., 2006; Logan and Nusse, 2004; Zhong et al., 2012). Compared with mammals, endochondral bone formation (*e.g.* ceratohyal) occurs first by differentiation of perichondral cells into osteoblasts that then forms a shell of bony mineralization (Eames et al., 2012; Hammond and Schulte-Merker, 2009; Jing et al., 2015; Paul et al., 2016). Here, we highlight the role of the non-canonical Wnt signaling pathway in temporal regulation of the endochondral ossification process.

Cartilage maturation and hypertrophy in an organized pattern is the core of endochondral bone formation. It requires chondrocytes to mature after proliferating and start producing collagen type 10 (Noonan et al., 1998). We showed that chondrocyte proliferation at around 6 dpf is most severely affected in *wls* mutants compared to the other mutants studied and concordant with previous mice studies (Maruyama et al., 2013). We also observed failure of chondrocyte differentiation in *wls* mutants, marked by the loss of *col10a1a* expression in the vast majority of craniofacial bones and cartilage and confirmed by the loss of *osterix* expression. Interestingly, we observed a high level of expression of *sox9a* and *runx2a* in *wls* mutant suggesting that cells remained in a pre-cartilage and pre-osteoblast stage but do not exit the cell cycle to mature. This step has been found to be key in hypertrophic chondrocytes becoming osteoblast during endochondral bone formation (Yang et al., 2014). Together, these observations indicate that chondrocyte failed to proliferate and osteoblasts failed to differentiate leading to defective bone formation. This points towards the essential role of *wls* regulating Wnt activity that is independent of *wnt9a* and *wnt5b* to direct chondrocyte proliferation, maturation and differentiation as well as osteogenesis. It may be the Wnt/β-catenin signaling acting through Wls that regulates this process. Indeed previous studies have showed that Wnt14, acting through the Wnt/β-catenin pathway enhances endochondral bone formation and promote chondrocyte maturation (Day et al., 2005). When *Wnt14* was overexpressed, chondrocytes differentiation was blocked and chondrocytes hypertrophy was inhibited evident through a downregulation of major matrix

metalloproteinase family members. Therefore it may be that Wnt14 acting through Wls would account for the defective endochondral phenotype observed.

While we did not observe any difference in proliferation in *wnt9a*, *wnt5b* or *gpc4* mutants, we did observe a loss of *col10a1a* and *osx* expression in the ceratohyal. This suggests that timely maturation and differentiation of chondrocytes is more prominent in the non-canonical Wnts. Previously published work on *gpc4* have described that a small proportion of *gpc4* −/− embryos survive to adulthood with robust formation of endochondral and dermal bones (LeClair et al., 2009). However, they noted the failure to form the symplectic bone, and describe other zebrafish mutants (*dackel* (*dak*) and *pinscher* (*pic*)) that also affects the biosynthesis of heparin sulfate proteoglycans resulting in a failure to form bones (Clement et al., 2008). Since we did not observe the formation of the ceratohyal, mentomeckelian or retroarticular in *gpc4* −/− at 8 dpf, a delay in chondrocyte maturation may be a contributory factor to the absence of endochondral ossification. The loss of endochondral bones in our *wnt5b* mutant is similar to *Wnt5a* and *Wnt5b* knockout mice where both have been shown to inhibit hypertrophic maturation by down regulating *Runx2* (Bradley and Drissi, 2010, 2011).

Disruption of Alizarin red staining in perichondral bones and loss of normal domains of *col10a1a* expression indicates that Wnt activity is required for normal bone formation along the endochondral pathway. We reason that the loss of cell polarity in the non-canonical Wnts may result in the inability for the overlying perichondral cells to receive appropriate signals from the underlying osterix-expressing chondrocytes. Previously studies have showed that *Indian hedgehog (Ihh)* is expressed in maturing chondrocytes while *Patched (Ptc)*, a Hh receptor and target of Hh signaling is expressed in the perichondrium (Avaron et al., 2006; Iwasaki et al., 1997; Vortkamp et al., 1996). Therefore, alignment of cilia may be crucial for perichondrial cells to receive *Ihh* signal from chondrocytes to initiate differentiation into osteoblasts. Indeed previous studies have shown that a high hedgehog signal leads to more osterix-expressing cells and perichondral osteoblasts (Hammond and Schulte-Merker, 2009). Therefore, polarization of cells through the non-canonical Wnt may be key in allowing the endochondral ossification process to proceed by aligning the cilia appropriately.

Along with the results of our study, we showed that *wls, wnt9a, wnt5b* and *gpc4* are all required for: 1) proper chondrocyte organization to shape the cartilage anlage and 2) timely chondrocyte maturation to initiate endochondral ossification. In contrast to the endochondral ossification process, *wls* additionally plays a key role in intramembranous ossification where osteoblasts directly differentiate from NCC-derived progenitors and do not require a pre-cartilage anlage (Fig. 8, Table 2). Since intramembranous bones are not affected in *wnt9a*, *wnt5b*, and *gpc4* mutants, it is likely that another ligand, perhaps *wnt14* acting through the β-catenin canonical Wnt pathway that requires *wls* for its secretion is essential for the commitment of NCC precursor cells to osteoblastic lineage. Therefore, the non-canonical Wnts acting through *wls* results in the loss of cell polarity and a delay in chondrocyte maturation, as seen in *wnt5b* and *wnt9a* mutants and confirmed with *gpc4* mutants. On the other hand, it is possible that the canonical Wnts acting through *wls* may account for the chondrocyte proliferative defect and severe loss of both endochondral and intramembranous bone.

In summary, we report the combined roles of *wls, wnt9a, wnt5b* and *gpc4* during zebrafish craniofacial cartilage and bone development by highlighting the interaction of these genes in juxtaposed cell types to regulate jaw morphogenesis. Further investigation focusing on the role of both canonical and non-canonical Wnts in the gene regulatory networks that differentiates the midzone and body of Meckel's cartilage will provide new insights into the diverse jaw lengths and sizes across species, as well as understandings into mandibular malformations and disorders.

4. Materials and methods

4.1. Zebrafish

Adult fish and embryos were cared and maintained as described (Kimmel et al., 1995). Mutant lines (*gpc4*$^{hi1688Tg/+}$, *wnt5b*$^{hi2735bTg/+}$) were obtained from ZIRC and previously described (Rochard et al., 2016; Sisson et al., 2015). *wls*$^{c186/+}$ was provided and previously characterized by Marnie Halpern (John Hopkins University) (Kuan et al., 2015). One of the two previously generated CRISPR *wnt9a* mutant line (Rochard et al., 2016) with the following target sequence TGTCCATTCTGCCACTGACC and harboring a −4 bp deletion (allele c.114_117del) was used for this study. FAM-PCR genotyping primers used for this *wnt9a* line are: Forward 5′-AGATTCCAATGGCTGCGCCCACTTG-3′ and Reverse 5′-GAGAGATGGAACTGCACGCTGGAGG -3′ with a FAM modification on the forward primer. WT peak is observed at 345 bp while mutant peaks at 341 bp.

The following transgenic lines were used: Tg(*sox10*:GFP), Tg(*sox10*:mCherry) (Dougherty et al., 2013) Tg(*osteocalcin*:GFP) (Singh et al., 2012), and Tg(*osterix*:RFP-NTR) (Singh et al., 2012).

4.2. *In situ* hybridization

Whole-mount RNA *in situ* hybridization was performed as previously described on staged embryos with minor modification (Thisse and Thisse, 2008). Embryos were collected at the desired stages, fixed in 4% PFA, bleached with 1.5% H2O2/1.5% KOH and stored in methanol at −20 °C. Embryos were rehydrated, digested with 10 μg/mL Proteinase K for 30 mins (96 hpf embryos) and refixed in 4% PFA. Prehybridization was performed at 70 °C for at least 4 h and digoxigenin-labeled anti-sense riboprobes (Roche Applied Science, Penzberg, Germany) were then added and incubated overnight at 70 °C. Washes were performed the following day at 70 °C in graded solutions of hybridization mix and SSC to 0.2XSSC/0.1%Tween-20. Embryos were blocked in 1XMABT/10%BSA/2%FCS for at least an hour. After pre-blocking, embryos were transferred to an anti-dig (1:10,000)/blocking solution and incubated overnight at 4 °C. The following day, embryos were extensively washed in MABT and then in NTMT solution (60 mM Tris-HCL pH 9.5, 60 mM NaCl, 30 mM $MgCl_2$ and 0.1% Tween-20). NBT and BCIP were used to achieve staining. After staining, embryos were refixed in 4% PFA and dehydrated in 100% MeOH and stored in 70% glycerol. When assaying for differences in expression, the staining development was monitored carefully and stopped at exactly the same time. Primers used are listed in Supplementary Table 1.

4.3. Skeletal staining

Alcian blue staining was performed as previously described (Walker and Kimmel, 2007). Ventral cartilage structure was dissected and flat-mounted prior to imaging. For live Alizarin red S stain, embryos were incubated in 0.005% Alizarin Red S/0.01 M HEPES in E3 overnight at 28.5 °C, washed extensively in E3 prior to confocal imaging and Alizarin red fluorophore excited at 580 nm.

4.4. Chondrocyte measurements, cell count and statistical analysis

Meckel's cartilage width (W) was measured from the distance between opposing retroarticular processes and the length (L) was measured from the midline to the tip of the retroarticular process. At least 10 different Meckel's cartilages per mutant were used for measurement from different embryos. Chondrocyte cell count was calculated by adding the total number of cells on one-half of the Meckel's cartilage obtained from a flat-mounted Alcian blue image in 10 different embryos. A one-way ANOVA test was used to compare means of representative groups and where the p-value is significant, a Bonferroni's multiple comparison tests were performed to compare means of mutant embryos to wild-type embryos. When numbers were small, Kruskal-Wallis test with Dunn's multiple comparisons test was used to compare medians across various groups. Rose plots were generated from Oriana Statistical program.

4.5. BrdU assay and immunofluorescence

BrdU incorporation was performed as previously described with some modifications (Verduzco and Amatruda, 2011). 6 dpf embryos were pulsed with 15 mM of BrdU/10% dimethylsulfoxide in E3 (Sigma B5002) on ice for 20 min and chased for 4 h in warm E3 at 28.5 °C. Embryos were then fixed in 4% PFA and stored in methanol at −20 °C. Following rehydration in graded Methanol: PBST series, the embryos were digested in 10 μg/mL Proteinase K for 30 mins, washed in PBS/0.1%Triton-X (PBSTx) and refixed in 4% PFA for 20 mins. Embryos were then incubated in 2N HCL for 1 h, rinsed with PBSTx and incubated in blocking solution (10% donkey serum, 1X PBSTx) for at least 1 h before incubating in mouse anti-BrDU (1:400, Sigma B2531) overnight at 4 °C. Embryos were then washed all day with multiple changes of PBSTx and then incubated in secondary antibodies (donkey Alexa-Fluor-594 1:400 and conjugated anti-GFP Alexa Fluor 488 1:400) overnight. Following multiple PBSTx washes, embryos were stored in 35% glycerol/PBST at 4 °C. BrdU positive chondrocytes (yellow cells – *sox10*:GFP positive and BrdU (red) positive) were counted from confocal Z-stacks.

For muscle stain, Alexa Fluor-647 phalloidin 1:400 was used. For microtubule organizing centers, mouse anti-α-acetylated tubulin (1:200, Sigma T7451) was used and mouse Alexa-Fluor 594 1:400 for secondary staining.

4.6. Confocal imaging

Embryos on a Tg(*sox10*:GFP) background were imaged using Nikon Ai scanning confocal microscope, mounted in 3.5% methylcellulose-0.013% Tricaine. Multiple embryos were imaged and traced until 4 dpf when they reveal their phenotype. Embryos were additionally genotyped for confirmation.

4.7. Acridine orange

Apoptosis detection by acridine orange was performed as previously described (Verduzco and Amatruda, 2011). 6 dpf embryos were incubated in 2 μg/mL solution of acridine Orange (Sigma, A6014) in E3 for 30 min at room temperature. Embryos were subsequently washed extensively in E3, tricaine treated and mounted prior to confocal imaging.

Supplementary Material

Refer to Web version on PubMed Central for supplementary material.

Acknowledgments

We thank Drs. Jenna Galloway, Patty Purcell and Shannon Fisher for valuable discussions and comments on the manuscript. We thank Renee Ethier for fish care and Dr. Ken Poss for sharing the Tg(*osx*:RFP-NTR) and Tg(*osc*:GFP) lines.

Funding

This work was supported by National Institute of Dental and Craniofacial Research Grant R03DE024490 and by a grant from Shriners Hospital for Children to ECL.

References

Alexander C, Piloto S, Le Pabic P, Schilling TF. Wnt signaling interacts with bmp and edn1 to regulate dorsal-ventral patterning and growth of the craniofacial skeleton. PLoS Genet. 2014; 10:e1004479. [PubMed: 25058015]

Avaron F, Hoffman L, Guay D, Akimenko MA. Characterization of two new zebrafish members of the hedgehog family: atypical expression of a zebrafish indian hedgehog gene in skeletal elements of both endochondral and dermal origins. Dev Dyn: Off Publ Am Assoc Anat. 2006; 235:478–489.

Bird NC, Mabee PM. Developmental morphology of the axial skeleton of the zebrafish, Danio rerio (Ostariophysi: Cyprinidae). Dev Dyn: Off Publ Am Assoc Anat. 2003; 228:337–357.

Bradley EW, Drissi MH. WNT5A regulates chondrocyte differentiation through differential use of the CaN/NFAT and IKK/NF-kappaB pathways. Mol Endocrinol. 2010; 24:1581–1593. [PubMed: 20573686]

Bradley EW, Drissi MH. Wnt5b regulates mesenchymal cell aggregation and chondrocyte differentiation through the planar cell polarity pathway. J Cell Physiol. 2011; 226:1683–1693. [PubMed: 21413026]

Choe CP, Collazo A, Trinh le A, Pan L, Moens CB, Crump JG. Wnt-dependent epithelial transitions drive pharyngeal pouch formation. Dev Cell. 2013; 24:296–309. [PubMed: 23375584]

Clement A, Wiweger M, von der Hardt S, Rusch MA, Selleck SB, Chien CB, Roehl HH. Regulation of Zebrafish Skeletogenesis by ext2/dackel and papst1/pinscher. PLoS Genet. 2008; 4:e1000136. [PubMed: 18654627]

Clevers H, Nusse R. Wnt/beta-catenin signaling and disease. Cell. 2012; 149:1192–1205. [PubMed: 22682243]

Curtin E, Hickey G, Kamel G, Davidson AJ, Liao EC. Zebrafish wnt9a is expressed in pharyngeal ectoderm and is required for palate and lower jaw development. Mech Dev. 2011; 128:104–115. [PubMed: 21093584]

Day TF, Guo X, Garrett-Beal L, Yang Y. Wnt/beta-catenin signaling in mesenchymal progenitors controls osteoblast and chondrocyte differentiation during vertebrate skeletogenesis. Dev Cell. 2005; 8:739–750. [PubMed: 15866164]

Dougherty M, Kamel G, Grimaldi M, Gfrerer L, Shubinets V, Ethier R, Hickey G, Cornell RA, Liao EC. Distinct requirements for wnt9a and irf6 in extension and integration mechanisms during zebrafish palate morphogenesis. Development. 2013; 140:76–81. [PubMed: 23154410]

Eames BF, Amores A, Yan YL, Postlethwait JH. Evolution of the osteoblast: skeletogenesis in gar and zebrafish. BMC Evolut Biol. 2012; 12:27.

Eames BF, DeLaurier A, Ullmann B, Huycke TR, Nichols JT, Dowd J, McFadden M, Sasaki MM, Kimmel CB. FishFace: interactive atlas of zebrafish craniofacial development at cellular resolution. BMC Dev Biol. 2013; 13:23. [PubMed: 23714426]

Eames BF, Sharpe PT, Helms JA. Hierarchy revealed in the specification of three skeletal fates by Sox9 and Runx2. Dev Biol. 2004; 274:188–200. [PubMed: 15355797]

Fanto M, McNeill H. Planar polarity from flies to vertebrates. J Cell Sci. 2004; 117:527–533. [PubMed: 14730010]

Flores MV, Tsang VW, Hu W, Kalev-Zylinska M, Postlethwait J, Crosier P, Crosier K, Fisher S. Duplicate zebrafish runx2 orthologues are expressed in developing skeletal elements. Gene Expr Pattern: GEP. 2004; 4:573–581. [PubMed: 15261836]

Frommer J, Margolies MR. Contribution of Meckel's cartilage to ossification of the mandible in mice. J Dent Res. 1971; 50:1260–1267. [PubMed: 5285785]

Glass DA 2nd, Bialek P, Ahn JD, Starbuck M, Patel MS, Clevers H, Taketo MM, Long F, McMahon AP, Lang RA, Karsenty G. Canonical Wnt signaling in differentiated osteoblasts controls osteoclast differentiation. Dev Cell. 2005; 8:751–764. [PubMed: 15866165]

Guo X, Day TF, Jiang X, Garrett-Beal L, Topol L, Yang Y. Wnt/beta-catenin signaling is sufficient and necessary for synovial joint formation. Genes Dev. 2004; 18:2404–2417. [PubMed: 15371327]

Hammond CL, Schulte-Merker S. Two populations of endochondral osteoblasts with differential sensitivity to Hedgehog signalling. Development. 2009; 136:3991–4000. [PubMed: 19906866]

Hartmann C. A Wnt canon orchestrating osteoblastogenesis. Trends Cell Biol. 2006; 16:151–158. [PubMed: 16466918]

Hartmann C, Tabin CJ. Dual roles of Wnt signaling during chondrogenesis in the chicken limb. Development. 2000; 127:3141–3159. [PubMed: 10862751]

Hartmann C, Tabin CJ. Wnt-14 plays a pivotal role in inducing synovial joint formation in the developing appendicular skeleton. Cell. 2001; 104:341–351. [PubMed: 11239392]

Heisenberg CP, Tada M, Rauch GJ, Saude L, Concha ML, Geisler R, Stemple DL, Smith JC, Wilson SW. Silberblick/Wnt11 mediates convergent extension movements during zebrafish gastrulation. Nature. 2000; 405:76–81. [PubMed: 10811221]

Heuze Y, Singh N, Basilico C, Jabs EW, Holmes G, Richtsmeier JT. Morphological comparison of the craniofacial phenotypes of mouse models expressing the Apert FGFR2 S252W mutation in neural crest- or mesoderm-derived tissues. Bone. 2014; 63:101–109. [PubMed: 24632501]

Hill TP, Spater D, Taketo MM, Birchmeier W, Hartmann C. Canonical Wnt/beta-catenin signaling prevents osteoblasts from differentiating into chondrocytes. Dev Cell. 2005; 8:727–738. [PubMed: 15866163]

Hochgreb-Hagele T, Koo DE, Bronner ME. Znf385C mediates a novel p53-dependent transcriptional switch to control timing of facial bone formation. Dev Biol. 2015; 400:23–32. [PubMed: 25636963]

Ichikawa Y, Watahiki J, Nampo T, Nose K, Yamamoto G, Irie T, Mishima K, Maki K. Differences in the developmental origins of the periosteum may influence bone healing. J Periodontal Res. 2015; 50:468–478. [PubMed: 25225160]

Iwasaki M, Le AX, Helms JA. Expression of indian hedgehog, bone morphogenetic protein 6 and gli during skeletal morphogenesis. Mech Dev. 1997; 69:197–202. [PubMed: 9486541]

Jing Y, Zhou X, Han X, Jing J, von der Mark K, Wang J, de Crombrugghe B, Hinton RJ, Feng JQ. Chondrocytes directly transform into bone cells in mandibular condyle growth. J Dent Res. 2015; 94:1668–1675. [PubMed: 26341973]

Kague E, Gallagher M, Burke S, Parsons M, Franz-Odendaal T, Fisher S. Skeletogenic fate of zebrafish cranial and trunk neural crest. PloS One. 2012; 7:e47394. [PubMed: 23155370]

Kahn J, Shwartz Y, Blitz E, Krief S, Sharir A, Breitel DA, Rattenbach R, Relaix F, Maire P, Rountree RB, Kingsley DM, Zelzer E. Muscle contraction is necessary to maintain joint progenitor cell fate. Dev Cell. 2009; 16:734–743. [PubMed: 19460349]

Kimmel CB, Ballard WW, Kimmel SR, Ullmann B, Schilling TF. Stages of embryonic development of the zebrafish. Dev Dyn: Off Publ Am Assoc Anat. 1995; 203:253–310.

Krishnan V, Bryant HU, Macdougald OA. Regulation of bone mass by Wnt signaling. J Clin Investig. 2006; 116:1202–1209. [PubMed: 16670761]

Kronenberg HM. Developmental regulation of the growth plate. Nature. 2003; 423:332–336. [PubMed: 12748651]

Kuan YS, Roberson S, Akitake CM, Fortuno L, Gamse J, Moens C, Halpern ME. Distinct requirements for Wntless in habenular development. Dev Biol. 2015; 406:117–128. [PubMed: 26116173]

Le Pabic P, Ng C, Schilling TF. Fat-Dachsous signaling coordinates cartilage differentiation and polarity during craniofacial development. PLoS Genet. 2014; 10:e1004726. [PubMed: 25340762]

LeClair EE, Mui SR, Huang A, Topczewska JM, Topczewski J. Craniofacial skeletal defects of adult zebrafish Glypican 4 (knypek) mutants. Dev Dyn: Off Publ Am Assoc Anat. 2009; 238:2550–2563.

Logan CY, Nusse R. The Wnt signaling pathway in development and disease. Annu Rev Cell Dev Biol. 2004; 20:781–810. [PubMed: 15473860]

Maruyama T, Jiang M, Hsu W. Gpr177, a novel locus for bone mineral density and osteoporosis, regulates osteogenesis and chondrogenesis in skeletal development. J Bone Miner Res: Off J Am Soc Bone Miner Res. 2013; 28:1150–1159.

Miller CT, Yelon D, Stainier DY, Kimmel CB. Two endothelin 1 effectors, hand2 and bapx1, pattern ventral pharyngeal cartilage and the jaw joint. Development. 2003; 130:1353–1365. [PubMed: 12588851]

Mork L, Crump G. Zebrafish craniofacial development: a window into early patterning. Curr Top Dev Biol. 2015; 115:235–269. [PubMed: 26589928]

Nair S, Li W, Cornell R, Schilling TF. Requirements for Endothelin type-A receptors and Endothelin-1 signaling in the facial ectoderm for the patterning of skeletogenic neural crest cells in zebrafish. Development. 2007; 134:335–345. [PubMed: 17166927]

Nakayama N, Han CY, Cam L, Lee JI, Pretorius J, Fisher S, Rosenfeld R, Scully S, Nishinakamura R, Duryea D, Van G, Bolon B, Yokota T, Zhang K. A novel chordin-like BMP inhibitor, CHL2, expressed preferentially in chondrocytes of developing cartilage and osteoarthritic joint cartilage. Development. 2004; 131:229–240. [PubMed: 14660436]

Neuhauss SC, Solnica-Krezel L, Schier AF, Zwartkruis F, Stemple DL, Malicki J, Abdelilah S, Stainier DY, Driever W. Mutations affecting craniofacial development in zebrafish. Development. 1996; 123:357–367. [PubMed: 9007255]

Noonan KJ, Hunziker EB, Nessler J, Buckwalter JA. Changes in cell, matrix compartment, and fibrillar collagen volumes between growth-plate zones. J Orthop Res: Off Publ Orthop Res Soc. 1998; 16:500–508.

Nowlan NC, Murphy P, Prendergast PJ. A dynamic pattern of mechanical stimulation promotes ossification in avian embryonic long bones. J Biomech. 2008; 41:249–258. [PubMed: 18005973]

Olsen BR, Reginato AM, Wang W. Bone development. Annu Rev Cell Dev Biol. 2000; 16:191–220. [PubMed: 11031235]

Paul S, Schindler S, Giovannone D, de Millo Terrazzani A, Mariani FV, Crump JG. Ihha induces hybrid cartilage-bone cells during zebrafish jawbone regeneration. Development. 2016

Quarto N, Wan DC, Kwan MD, Panetta NJ, Li S, Longaker MT. Origin matters: differences in embryonic tissue origin and Wnt signaling determine the osteogenic potential and healing capacity of frontal and parietal calvarial bones. J Bone Miner Res: Off J Am Soc Bone Miner Res. 2010; 25:1680–1694.

Rochard L, Monica SD, Ling IT, Kong Y, Roberson S, Harland R, Halpern M, Liao EC. Roles of Wnt pathway genes wls, wnt9a, wnt5b, frzb and gpc4 in regulating convergent-extension during palate morphogenesis. Development. 2016

Rodda SJ, McMahon AP. Distinct roles for Hedgehog and canonical Wnt signaling in specification, differentiation and maintenance of osteoblast progenitors. Development. 2006; 133:3231–3244. [PubMed: 16854976]

Savostin-Asling I, Asling CW. Resorption of calcified cartilage as seen in Meckel's cartilage of rats. Anat Rec. 1973; 176:345–359. [PubMed: 4716419]

Schilling TF, Kimmel CB. Segment and cell type lineage restrictions during pharyngeal arch development in the zebrafish embryo. Development. 1994; 120:483–494. [PubMed: 8162849]

Schilling TF, Kimmel CB. Musculoskeletal patterning in the pharyngeal segments of the zebrafish embryo. Development. 1997; 124:2945–2960. [PubMed: 9247337]

Semenov MV, Habas R, Macdonald BT, He X. SnapShot: noncanonical Wnt signaling pathways. Cell. 2007; 131:1378. [PubMed: 18160045]

Sepich DS, Usmani M, Pawlicki S, Solnica-Krezel L. Wnt/PCP signaling controls intracellular position of MTOCs during gastrulation convergence and extension movements. Development. 2011; 138:543–552. [PubMed: 21205798]

Shwartz Y, Farkas Z, Stern T, Aszodi A, Zelzer E. Muscle contraction controls skeletal morphogenesis through regulation of chondrocyte convergent extension. Dev Biol. 2012; 370:154–163. [PubMed: 22884393]

Singh SP, Holdway JE, Poss KD. Regeneration of amputated zebrafish fin rays from de novo osteoblasts. Dev Cell. 2012; 22:879–886. [PubMed: 22516203]

Sisson BE, Dale RM, Mui SR, Topczewska JM, Topczewski J. A role of glypican4 and wnt5b in chondrocyte stacking underlying craniofacial cartilage morphogenesis. Mech Dev. 2015; 138(Pt 3):279–290. [PubMed: 26459057]

Spater D, Hill TP, O'Sullivan R, Gruber J, Conner M, Hartmann C, DA. Wnt9a signaling is required for joint integrity and regulation of Ihh during chondrogenesis. Development. 2006; 133:3039–3049. [PubMed: 16818445]

Storm EE, Kingsley DM. GDF5 coordinates bone and joint formation during digit development. Dev Biol. 1999; 209:11–27. [PubMed: 10208739]

Thisse C, Thisse B. High-resolution in situ hybridization to whole-mount zebrafish embryos. Nat Protoc. 2008; 3:59–69. [PubMed: 18193022]

Topczewski J, Dale RM, Sisson BE. Planar cell polarity signaling in craniofacial development. Organogenesis. 2011; 7:255–259. [PubMed: 22134372]

Verduzco D, Amatruda JF. Analysis of cell proliferation, senescence, and cell death in zebrafish embryos. Methods Cell Biol. 2011; 101:19–38. [PubMed: 21550438]

Vortkamp A, Lee K, Lanske B, Segre GV, Kronenberg HM, Tabin CJ. Regulation of rate of cartilage differentiation by Indian hedgehog and PTH-related protein. Science. 1996; 273:613–622. [PubMed: 8662546]

Walker MB, Kimmel CB. A two-color acid-free cartilage and bone stain for zebrafish larvae. Biotech Histochem: Off Publ Biol Stain Comm. 2007; 82:23–28.

Wu BT, Wen SH, Hwang SP, Huang CJ, Kuan YS. Control of Wnt5b secretion by Wntless modulates chondrogenic cell proliferation through fine-tuning fgf3 expression. J Cell Sci. 2015; 128:2328–2339. [PubMed: 25934698]

Yan YL, Miller CT, Nissen RM, Singer A, Liu D, Kirn A, Draper B, Willoughby J, Morcos PA, Amsterdam A, Chung BC, Westerfield M, Haffter P, Hopkins N, Kimmel C, Postlethwait JH. A zebrafish sox9 gene required for cartilage morphogenesis. Development. 2002; 129:5065–5079. [PubMed: 12397114]

Yang L, Tsang KY, Tang HC, Chan D, Cheah KS. Hypertrophic chondrocytes can become osteoblasts and osteocytes in endochondral bone formation. Proc Natl Acad Sci USA. 2014; 111:12097–12102. [PubMed: 25092332]

Yang Y, Topol L, Lee H, Wu J. Wnt5a and Wnt5b exhibit distinct activities in coordinating chondrocyte proliferation and differentiation. Development. 2003; 130:1003–1015. [PubMed: 12538525]

Zhong Z, Zylstra-Diegel CR, Schumacher CA, Baker JJ, Carpenter AC, Rao S, Yao W, Guan M, Helms JA, Lane NE, Lang RA, Williams BO. Wntless functions in mature osteoblasts to regulate bone mass. Proc Natl Acad Sci USA. 2012; 109:E2197–E2204. [PubMed: 22745162]

Appendix A. Supplementary material

Supplementary data associated with this article can be found in the online version at doi: 10.1016/j.ydbio.2016.11.016.

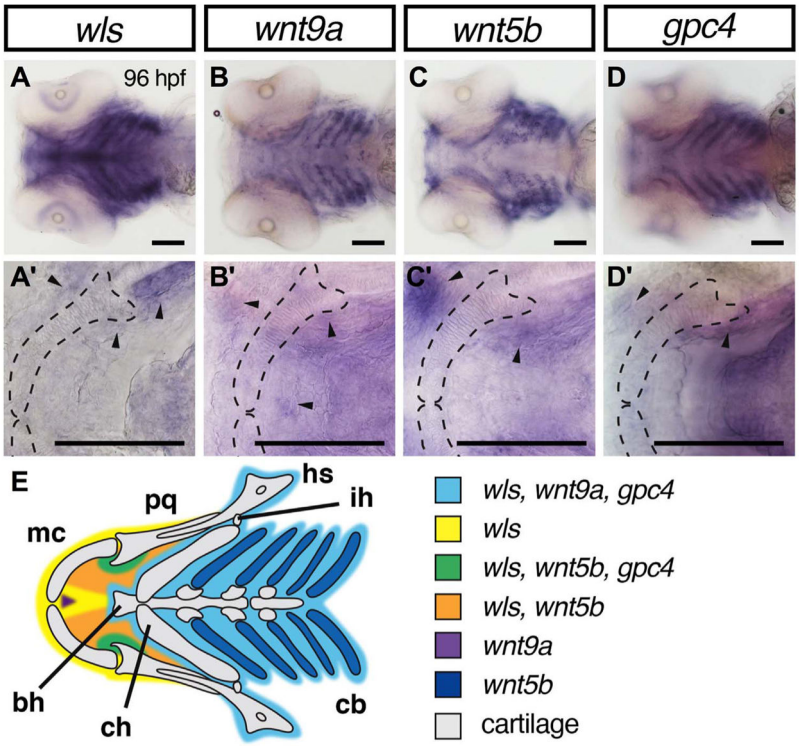

Fig. 1.

Overlapping domains of gene expression of *wls*, *wnt9a*, *wnt5b* and *gpc4* in ventral craniofacial cartilages. (**A–D**) 10X Whole mount RNA *in situ* hybridization with ventral views with 40X focused on Meckel's cartilage **(A′–D′).** At 96 hpf, *wls* (**A**) is expressed in the surrounding tissue including Meckel's cartilage and co-expressed with *wnt9a* (**B**) and *gpc4* (**D**) in the posterior ceratobranchials (light blue). In contrast, *wnt5b* appeared to be expressed in the chondrocytes of the ceratobranchials and the blood vessels surrounding them (**C**). *wls, wnt5b* and *gpc4* co-localized in the surrounding mesenchyme around the jaw joint (arrowheads in A′–D′ and green in diagram E). *wnt5b* is expressed in the oral epithelium with *wls*. There is discrete expression of *wnt9a* in the anterior midline (purple) adjacent to the intermandibulare anterior muscle. Annotation: Meckel's cartilage (mc), palatoquadrate (pq), hyosymplectic (hs), interhyal (ih), ceratobranchial (cb), ceratohyal (ch), basihyal (bh). Scale=50 μm.

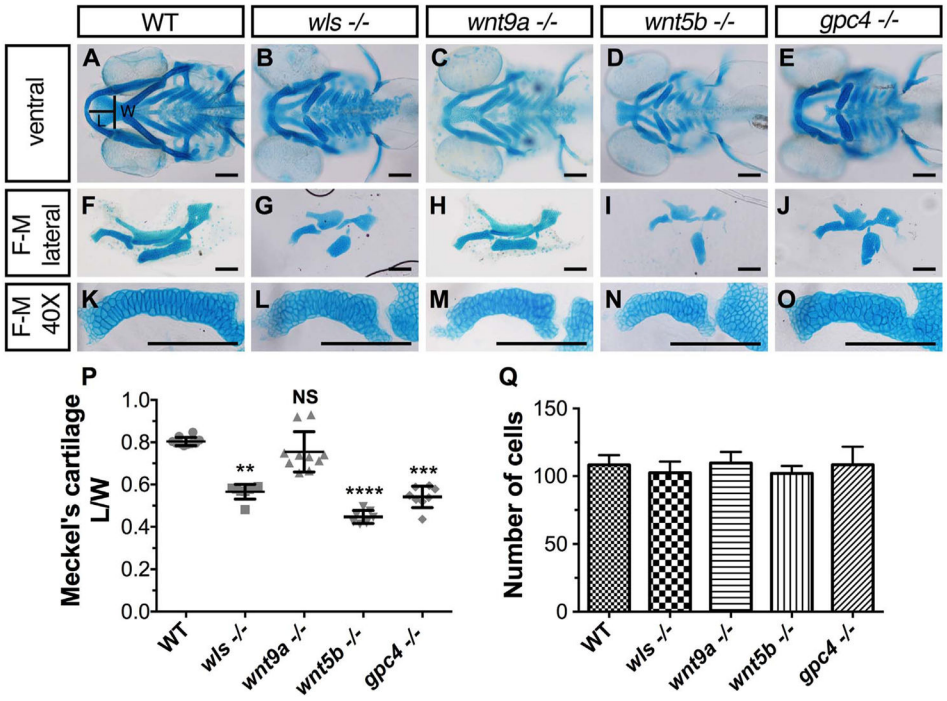

Fig. 2.

Cartilage morphogenetic defects in *wls*, *wnt9a*, *wnt5b* and *gpc4* mutants. (**A–E**) Ventral view of whole-mount 96 hpf Alcian blue stain of *wls*, *wnt9a*, *wnt5b* and *gpc4*. (**F–J**) Dissected flat-mounted lateral image of ventral cartilages. (**K–O**) 40X image of the Meckel's cartilage lateral view. Length (L) calculated from the midline tip of the Meckel's cartilage to the middle of the imaginary line (width (W)) between the retroarticular processes. (**P**) Meckel's cartilage length/width ratio measured from a clutch of imaged embryos (**p < 0.01, ***p < 0.001, ****p < 0.0001; Kruskal-Wallis test with Dunn's multiple comparison test. Significance level at p < 0.05). (**Q**) Number of cells from one-half of Meckel's cartilage was counted from figures K–O. No statistically significant difference in cell number across *wls*, *wnt9a*, *wnt5b* and *gpc4* (p=0.1151, NS; One-way ANOVA). Scale =50 μm..

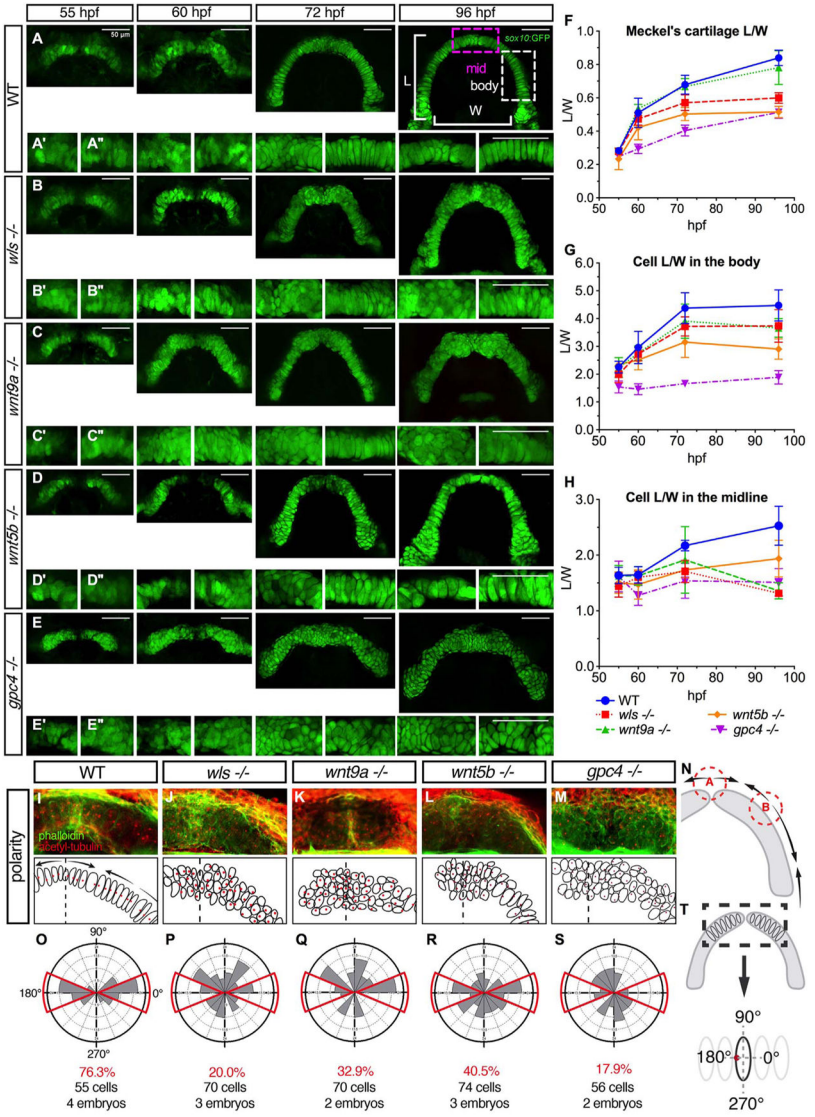

Fig. 3.

Distinct cellular and polarity differences between midzone and body of Meckel's cartilage in *wls*, *wnt9a*, *wnt5b* and *gpc4* mutants. (A–E) Wnt gene were crossed to Tg(*sox10*:GFP) transgenic line and homozygote embryos were imaged at difference time points starting at 55 hpf when convergence of the Meckel's cartilage occurs until 96 hpf when the arch is complete. Defects evident from 60 hpf especially in *gpc4* −/− and by 72 hpf, obvious midline defect was seen in *wls, wnt9a* and *gpc4* and body defects apparent in *gpc4. wnt5b* exhibited a smaller cartilage size throughout morphogenesis. (A; 96 hpf) Graphical representation of the L/W measurements from Meckel's cartilage. (A′) 20X image of Meckel's cartilage in the midline and (A″) 20X image of the body of Meckel's. (F–H) Individual cell length/width ratio were measured and plotted over time from 2 distinct parts of the Meckel's; midzone and body as marked in the illustration. (I–M) 72 hpf WT and homozygote embryos were stained for actin with phalloidin (green) to delineate cell membranes and acetylated-tubulin (red) to reveal microtubule organizing center (MTOC).

(N) Polarity pattern for Meckel's cartilage at 72 hpf showing 2 inflection points; point A where the hemi-Meckel's cartilage meet in the midline and point B within the body of each hemi-Meckel's cartilage. (O–S) Rose plots of cell polarity as indicated by MTOC measured from cells within the midzone portion of Meckel's cartilage. (T; black dotted box). Scale=50 μm.

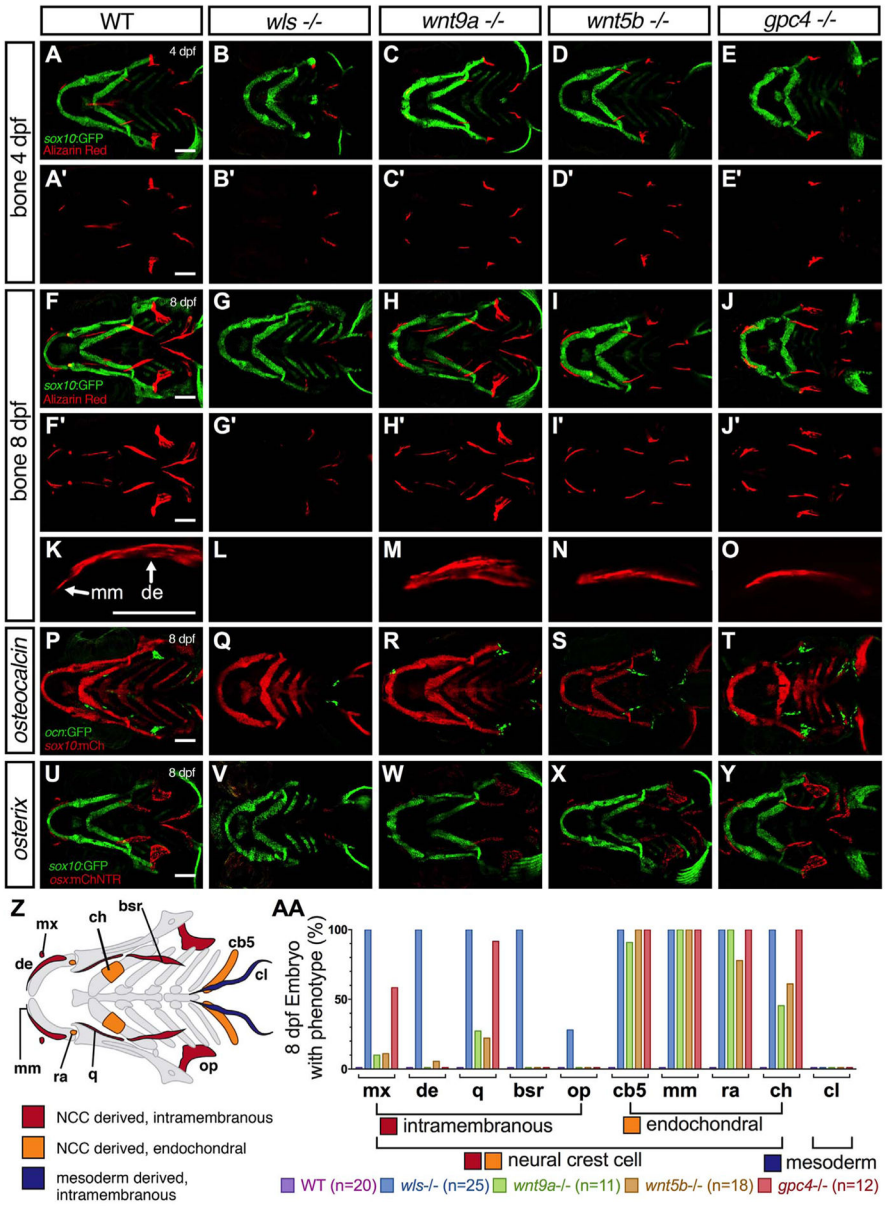

Fig. 4.

Bone defects in *wls*, *wnt9a*, *wnt5b* and *gpc4* mutants. (**A–J**) Maximum intensity projections of live confocal imaging stacks of 4 dpf (**A–E**) and 8 dpf (**F–J**) Wnt homozygotes in Tg(*sox10*:GFP) background stained with alizarin red S. **(K–O)** 40X confocal maximum intensity projections of alizarin red stain focusing on the dentary bone (de) and mentomeckelian (mm). The mentomeckelian is seen as a flatter bone attached to the distal end of the dentary that is thicker. A clear boundary is observed between the mm and de. *wls* mutants lacks the dentary or mentomeckelian. (**P–T**) Confocal maximum intensity projections of *osteocalcin* transgene expression in Wnt mutants in a Tg(*sox10*:mCherry) background. (**U–Y**) Confocal maximum intensity projections of *osx* transgene expression in Wnt mutants in a Tg(*sox10*:GFP) background. (**Z**) Graphical map of neural-crest cell

(NCC)-derived bone (red; intramembranous ossification and orange; endochondral ossification) and mesoderm derived bone (blue). Mentomeckelian (mm), Maxilla (mx), Dentary (de), retroarticular (ra), quadrate (q), ceratohyal (ch), branchiostegal rays (bsr), opercle (op), ceratobranchial 5 (cb5), cleithrum (cl). (**AA**) Percentage of mutant with bony phenotype of different bones in the craniofacial region where 100% indicates that all mutant embryos do not have that particular bone. Scale=50 μm.

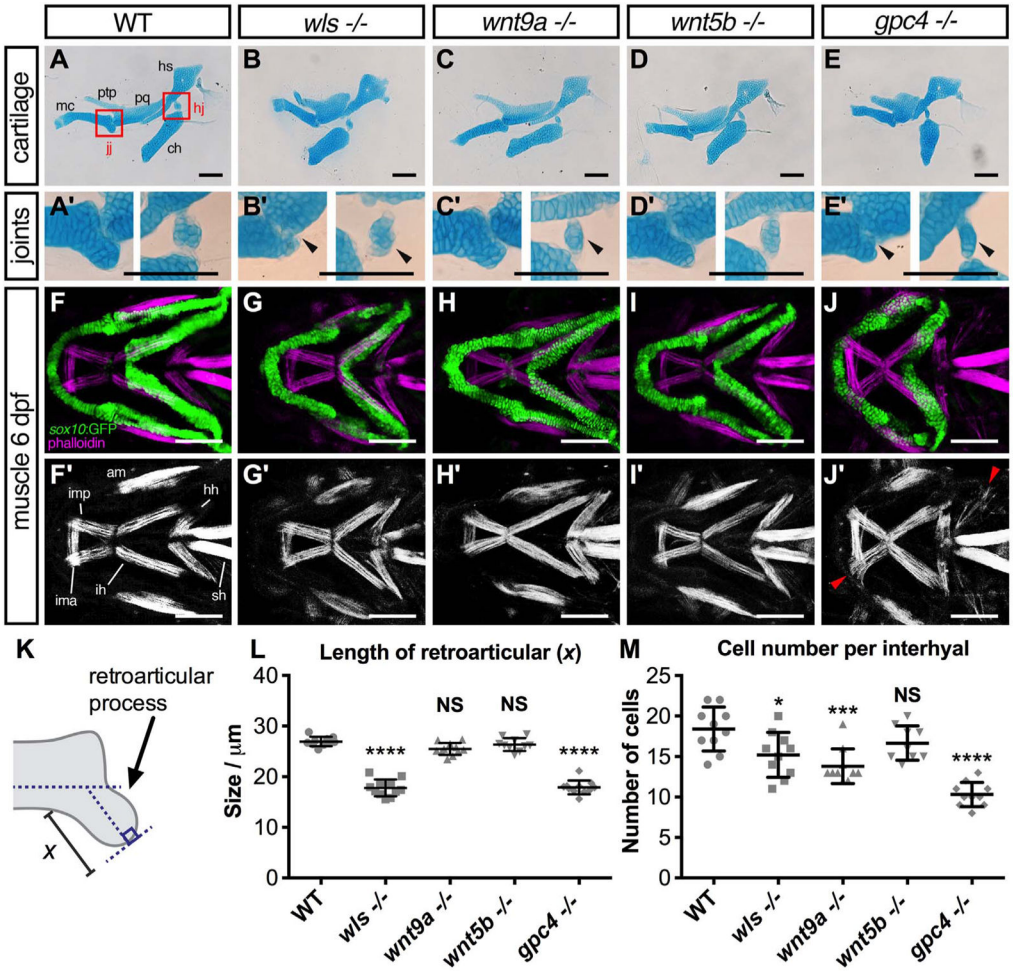

Fig. 5.

Joint and muscle defects in *wls*, *wnt9a*, *wnt5b*, and *gpc4* mutants. (**A–E**) Alcian blue stained ventral cartilage lateral whole-mounts of 8 dpf embryos and 40X zoomed image in **A′–E′** of the jaw joint (jj; left) and hinge joint (hj; right). Meckel's cartilage (mc), pterygoid process (ptp), palatoquadrate (pq), hyosymplectic (hs), and ceratohyal (ch). Jaw joint defects evident in *wls* and *gpc4* mutant whilst *wnt9a* exhibited a slightly malformed retroarticular process. *wls* displayed a clump of cells within the hinge-joint compared to the neatly stacked layered chondrocytes in wild-type. In contrast, *wnt9a, wnt5b* and *gpc4* were only a single cell layer in thickness. (**F–J**) Maximum intensity projections of 20X zoom confocal stacks showing muscle stain with phalloidin (purple) and anti-GFP (green) for cartilage elements. Muscle length defects apparent in all *Wnt* mutants with *gpc4* displaying disorganized intermandibularis posterior (imp) invading the gaps in Meckel's cartilage. Adductor mandibulae (am), intermandibularis anterior (ima), intermandibularis posterior (imp), hyohyoideus (hh), interhyoideus (ih), sternohyoides (sh) F′–J″ Single channel phalloidin flourescence. **(K)** Graphical representation of retroaritcular measurement. **(L)** Measured length of retroarticular process and **(M)** cell count per interhyal in WT and Wnt mutants. (*p < 0.01***p < 0.001, ****p < 0.0001; Kruskal-Wallis test with Dunn's multiple comparison test. Significance level at $p < 0.05$). Scale =50 µm..

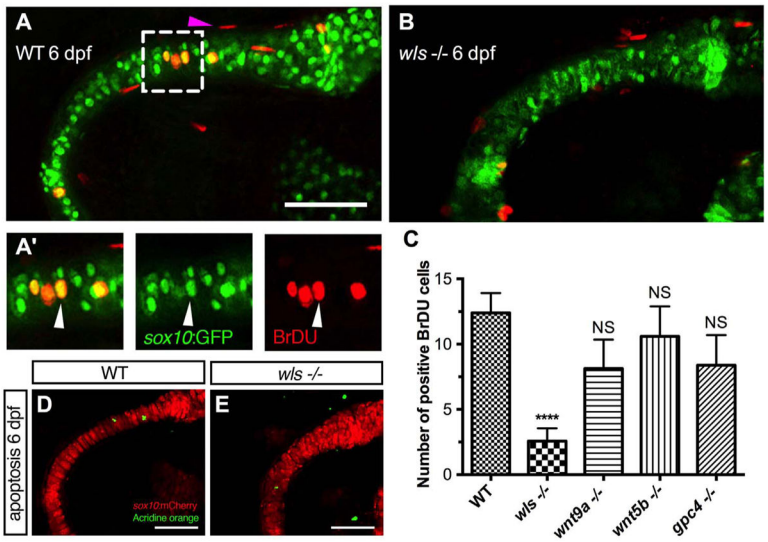

Fig. 6.

Chondrocyte proliferation defect in *wls* mutant precedes the differentiation defect. (**A, B**) Representative BrdU assay confocal stacked image in WT 6 dpf (**A**) and *wls* −/− (**B**) embryo with zoomed views of WT BrdU (red) colocalizing with chondrocytes (**A′**) in the Meckel's cartilage (green). Arrowhead points to a representative chondrocyte that expressed both *sox10* and BrdU and used for quantification. (**C**) Quantification of BrdU positive cells in Wnt mutants. Proliferation significantly differed in *wls* −/− compared to WT (****$p < 0.001$; Kruskal-Wallis test and Dunn's multiple comparison test, NS = not significant). (**D, E**) No difference in chondrocyte apoptosis as showed with Acridine orange live staining at 6 dpf in *wls* −/−. Scale=50 μm.

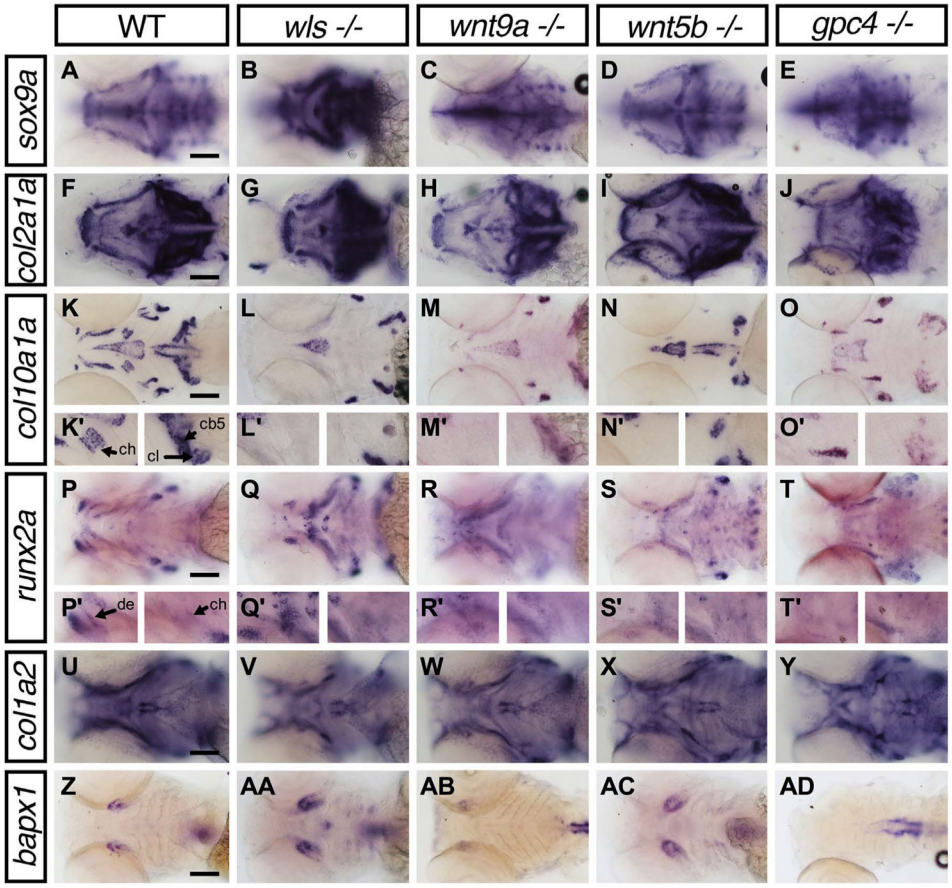

Fig. 7.

Lower jaw gene expression pattern of chondrocyte and bone markers in *wls*, *wnt9a*, *wnt5b* and *gpc4* mutants. Whole-mount RNA *in situ* hybridization of chondrocyte differentiation markers; *sox9a* (**A–E**) and chondrocyte matrix; *col2a1* (**F–J**). Hypertrophic chondrocyte marker; *col10a1a* (**K–O**), Bone and tendon marker; *col1a2* (**P–T**), osteoblastic progenitor marker; *runx2a* (**U–Y**) and joint marker; *bapx1* (**Z–AD**). **(K′–L′)** 40X image focused on ceratohyal (ch; left) and both cleithrum and ceratobranchial 5 (cl, cb; right). (P′–T′) 40X images focused on dentary (de; left) and ceratohyal (right). Apparent increase in *sox9a, runx2a* expression pattern in *wls* −/− with concomitant loss of *col10a1a*. Black arrowhead points to the position of Meckel's cartilage. Scale=50 μm..

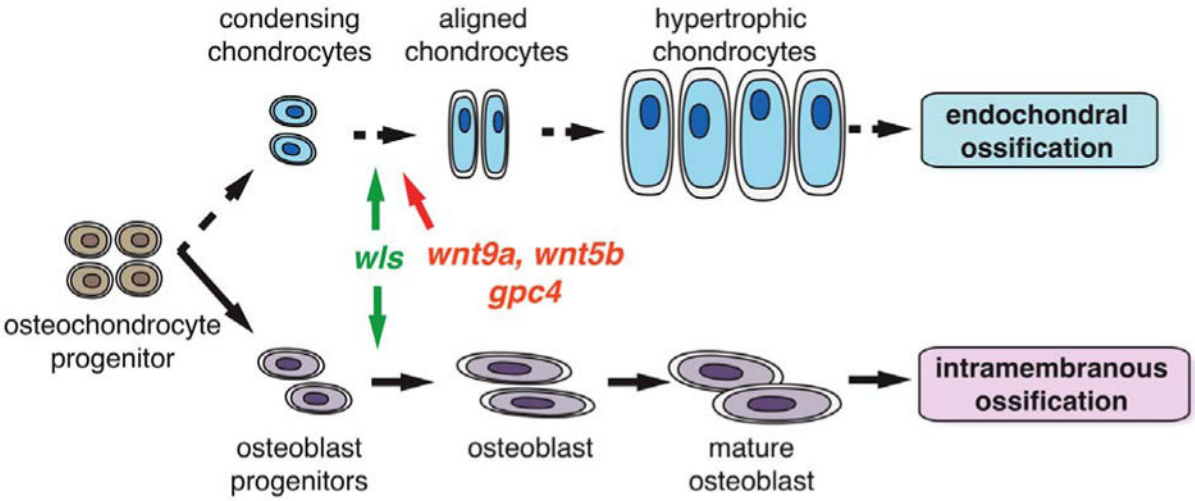

Fig. 8.

Summary diagram indicating role of *wls*, *wnt9a*, *wnt5b* and *gpc4* in endochondral and intramembranous ossification process. *wls* drives both endochondral and intramembranous process while *wnt9a*, *wnt5b* and *gpc4* have a more prominent roles in the endochondral process.

Table 1

Summary gene expression comparison within the Meckel's cartilage.

Markers in visercocranium		***wls* −/−**	***wnt9a* −/−**	***wnt5b* −/−**	***gpc4* −/−**
Chondrogenesis	*sox9a*	++	+	+	+
ECM remodeling	*collagen type 2a1*	+	+	+	+
ECM remodeling	*collagen type 10a1a*	−	+	−	+
ECM remodeling	*collagen type 1a2*	−	+	−	+
Osteogenesis	*runx2a*	++	+	+	++
Joint patterning	*bapx1*	++	+/−	+	−

Qualitative scoring of whole-mount RNA *in situ* hybridization expression patterns compared with their WT sibling within a given clutch. Annotation: '++' = high detectable expression, '+' = normal expression, '+/− ' = low detectable expression and '− ' = undetectable expression.

Table 2

Summary gene requirements in ventral cartilage development.

Processes	*wls*	*wnt9a*	*wnt5b*	*gpc4*
Chondrocyte polarity and orientation	+	+	+	+
Chondrocyte proliferation	+	−	−	−
Chondrocyte maturation/hypertrophy	+	+	+	+
Articular cartilage	+	+	+	+
Endochondral ossification	+	+	+	+
Intramembranous ossification	+	−	−	−
Muscle	−	−	−	+

+= required, − = not required.